Directional Analysis of Images with Gabor Wavelets

R.M. RANGAYYAN[1], R.J. FERRARI[1,2], J.E.L. DESAUTELS[1,3], A.F. FRÈRE[2,4]

[1]Department of Electrical and Computer Engineering, University of Calgary, Calgary, Alberta, Canada, T2N 1N4.
ranga@enel.ucalgary.ca
[2]Department of Electrical Engineering, University of São Paulo, São Carlos, SP, 13560-250, Brazil.
ricardof@sel.eesc.sc.usp.br
[3]Alberta Cancer Board, Calgary, Alberta, Canada, T2P 3G9
[4]Nucleus of Science and Technology, University of Mogi das Cruzes, Mogi das Cruzes, SP, Brazil.

Abstract. This paper presents a new scheme for analysis of linear directional components in images by using a multiresolution representation based on Gabor wavelets. A dictionary of Gabor filters with varying tuning frequency and orientation, specifically designed in order to reduce the redundancy in the wavelet–based representation, is applied to the given image. The filter responses for different scales and orientation are analyzed by using the Karhunen–Loève (KL) transform and Otsu's method of thresholding. The KL transform is applied to select the principal components of the filter responses, preserving only the most relevant directional elements appearing at all scales. The first N principal components, thresholded by using Otsu's method, are used to reconstruct the magnitude and phase of the directional components of the image. In this work, Rose diagrams computed from the phase images are used for quantitative and qualitative analysis of the oriented patterns. The proposed scheme is applied to the analysis of asymmetry between left and right mammograms. For this purpose, a set of three features is extracted from the Rose diagrams and used in a parametric statistical classifier. A total of 80 images from 20 normal cases, 14 asymmetric cases, and 6 distortion cases from the Mini–MIAS database were used to evaluate the scheme using the leave–one–out methodology, resulting in an average diagnostic accuracy of 72.5%.

1 Introduction

Most of the concepts used in image processing and computer vision for oriented pattern analysis have their roots in neurophysiological studies of the mammalian visual system. Campbell and Robson [1] proposed that the human visual system decomposes retinal images into a number of filtered images, each of which contains intensity variations over a narrow range of frequency and orientation. Marcelja [2] and Jones and Palmer [3] demonstrated that simple cells in the primary visual cortex have receptive fields that are restricted to small regions of space and are highly structured, and that their behavior corresponds to local measurements of frequency.

According to Daugman [4], [5], one suitable model of the two–dimensional (2–D) receptive field profiles measured experimentally in mammalian cortical simple cells is the parameterized family of 2–D Gabor filters. Jones and Palmer [3] and Daugman [4] showed that a majority of cortical cells have 2–D receptive field profiles that can be well fit, in the sense of a statistical test, by members of the family of 2–D Gabor elementary functions. Another important characteristic of Gabor filters is their optimal joint resolution in both space and frequency, which suggests that Gabor filters are appropriate operators for tasks requiring simultaneous measurement in the two domains [6]. Except for the optimal joint resolution possessed by the Gabor functions, the difference of Gaussian (DOG) and difference of offset Gaussian (DOOG) filters used by Malik and Perona [7] have similar properties.

Gabor filters have been presented in several works on image processing [6], [8], [9]; however, most of these works are related to texture segmentation and analysis. Rolston and Rangayyan [10] proposed methods for analysis of directional linear components in images using multiresolution Gabor filters.

Inspired by the studies mentioned above, we propose a new scheme based on a Gabor wavelet approach to analyze directional components of images. The method is used to detect asymmetry in the fibro–glandular discs of left and right mammograms.

2 Construction of Gabor Wavelets

A 2–D Gabor function is a Gaussian modulated by a sinusoid. It is a nonorthogonal wavelet, and can be specified by the frequency of the sinusoid W and the standard deviations of the Gaussian σ_x and σ_y as

$$g(x,y) = \frac{1}{2\pi\sigma_x\sigma_y} \exp\left[-\frac{1}{2}\left(\frac{x^2}{\sigma_x^2} + \frac{y^2}{\sigma_y^2}\right) + 2\pi jWx\right] \quad (1)$$

0-7695-0878-2/00 $10.00 © 2000 IEEE

Despite this simple form, there is no standard and precise definition of a 2–D Gabor function, with several variations appearing in the literature [11],[8],[9]. In this work, we use the version of the Gabor wavelets proposed by Manjunath and Ma [12]. The Gabor wavelets in this representation are obtained by dilation and rotation of $g(x, y)$ as above by using the generating function

$$g_{mn}(x,y) = a^{-m} g(x', y'), \quad a > 1, \quad m, n = integers, \tag{2}$$

$$x' = a^{-m}(x\cos\theta + y\sin\theta)\ ,$$

$$y' = a^{-m}(-x\sin\theta + y\cos\theta)\ ,$$

where $\theta = n\pi/K$ with m and n indicating the scale and orientation, respectively. K is the total number of orientations desired. The scale factor a^{-m} in Equation 2 is meant to ensure that the energy is independent of m. Examples of Gabor wavelets are shown in Figure 1.

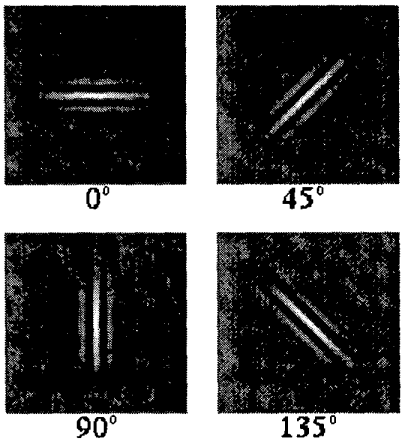

Figure 1: Examples of Gabor wavelets in the spatial domain with four orientations ($\theta = 0^o$, 45^o, 90^o, and 135^o) and one scale ($\sigma_x = 5$ and $\sigma_y = 16$ pixels). The size of each wavelet image shown is 121 × 121 pixels.

Equation 1 can be written in the frequency domain as

$$G(u,v) = \frac{1}{2\pi\sigma_u\sigma_v} \exp\left\{-\frac{1}{2}\left[\frac{(u-W)^2}{\sigma_u^2} + \frac{(v-W)^2}{\sigma_v^2}\right]\right\}, \tag{3}$$

where $\sigma_u = \frac{1}{2\pi\sigma_x}$ and $\sigma_v = \frac{1}{2\pi\sigma_y}$. The design strategy is used to project the filters so as to ensure that the half-peak magnitude supports of the filter responses in the frequency spectrum touch one another, as shown in Figure 2. Existing methods in the literature use either complex-valued Gabor filters [11] or pairs of Gabor filters with quadrature-phase relationship [6]. In this work, the representation uses real-valued filters oriented over a range of 180^o only, as opposed to the full 360^o range commonly described in the literature. Since the Gabor filters are used to extract meaningful features from real images (and hence with Hermitian frequency response [13]), the response to the even-symmetric filter component will remain unchanged for filters oriented 180^o out of phase and the odd-symmetric component will be negated. Thus, based upon this fact and on psychophysical grounds provided by Malik and Perona [7], we ignored half of the orientations in this work, as illustrated in Figure 2.

The proposed approach results in the following formulas for computing the filter parameters σ_u and σ_v :

$$a = \left(\frac{U_h}{U_l}\right)^{\frac{1}{S-1}},$$

$$\sigma_u = \frac{(a-1)U_h}{(a+1)\sqrt{2\ln 2}},$$

$$\sigma_v = \frac{\tan(\frac{\pi}{2K})\left[U_h - (\frac{\sigma_u^2}{U_h})2\ln 2\right]}{\sqrt{2\ln 2 - \frac{(2\ln 2)^2\sigma_u^2}{U_h^2}}}, \tag{4}$$

where U_l and U_h denote the lower and upper center frequencies of interest. The K and S parameters are, respectively, the number of orientations and the number of scales in the desired multiresolution decomposition procedure. The sinusoid frequency W is set equal to U_h, and $m = 0, 1, \ldots, S-1$. In order to ensure that the filters do not respond to regions with constant intensity, we have set the gain of each filter at $(u, v) = (0, 0)$ to zero.

3 Directional Analysis

The procedure proposed for analyzing directional components starts by computing a dictionary of Gabor filters according to the representation described in Section 2. In the present work, the Gabor wavelets were projected by using four scales ($S = 4$) and twelve directions ($K = 12$) with the lower and upper center frequencies specified as $U_l = 0.05$ and $U_h = 4.5$ cycles/pixel, respectively. The filtering process was performed in the frequency domain.

The filter outputs for each orientation and the four scales were analyzed by using the Karhunen–Loève (KL) transform [14]. The KL transform was used to select the principal components of the filter outputs, preserving only the most relevant directional elements present in all the scales. Results were then combined as illustrated in Figure 3 in order to allow the formation of an S-dimensional vector ($\overline{x}$)

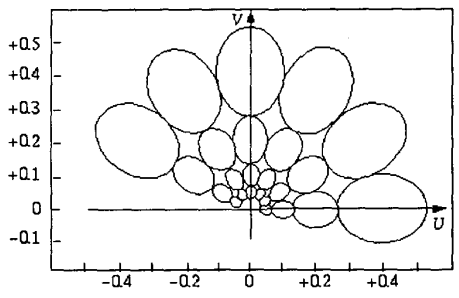

(a)

Figure 2: Typical Gabor filter design in the frequency domain (four scales, six orientations). Each ellipse represents the range of the corresponding filter response from 0.5 to 1.0 in squared magnitude.

for each pixel from each set of the corresponding pixels in the filtered images ($S = 4$, as mentioned above, is the number of scales used in the present work).

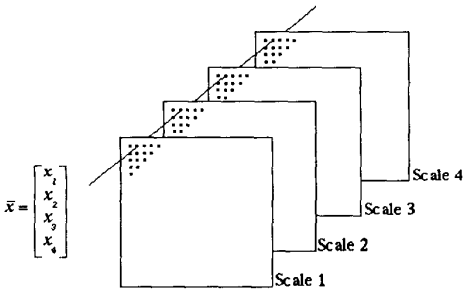

Figure 3: Formation of the vector $\overline{x}$ from the corresponding pixels of the same orientation and four different scales. The size of each image is 512 × 512 pixels.

The vectors corresponding to each position in the filter responses were used to compute the mean vector ($\overline{\mu}$) and the covariance matrix ($\overline{C}$). The eigenvalues and eigenvectors of the covariance matrix were then computed and arranged in descending order in a matrix $\overline{A}$ so that the first row of $\overline{A}$ is the eigenvector corresponding to the largest eigenvalue, and the last row is the eigenvector corresponding to the smallest eigenvalue. The first N principal components corresponding to 95% of the total variance were then selected and used to represent the oriented components in each specific orientation. The principal components were computed as $\overline{y} = \overline{A}(\overline{x} - \overline{\mu})$. Analysis of the variance was performed by evaluating the eigenvalues of the matrix $\overline{A}$. The KL method is optimal in the sense that it minimizes the mean squared error between the vectors $\overline{x}$ and their resulting approximations $\overline{y}$ [14]. The result of application of the KL transform to all orientations, as described above, is a set of K images, where K is the number of orientations.

Since the Gabor wavelets are nonorthogonal functions, they do not have a perfect reconstruction condition. This fact results in a small amount of out-of-band energy interfering with the reconstruction, which is translated into artifacts in the reconstructed image. In order to eliminate these artifacts, the images resulting from the KL transform were thresholded by using the maximum of Otsu's threshold values [15] computed for the K images. Otsu's method is a nonparametric technique for automatic threshold selection, and selects an optimal threshold value which maximizes the separability of the resultant classes.

Finally, the phase and magnitude images were composed by vector summation of the K filtered images [13].

4 Analysis of Asymmetry in Mammograms

Asymmetry between the left and right mammograms is an important sign used by radiologists to diagnose breast cancer [16]. Analysis of asymmetry can provide clues about the presence of early signs of tumors (parenchymal distortion, small asymmetric bright spots and contrast, etc.) that are not evaluated by other methods [17]. Several works have been presented in the literature addressing this problem [18], [19], [17], [20], [21]. Most of them applying some type of alignment of the breast images before performing asymmetry analysis. However, alignment procedures applied to mammograms have to confront many difficult problems such as the natural asymmetry of the breasts, absence of good corresponding points between the left and right breast images to perform matching, and distortions inherent to breast imaging.

A systematic anatomical approach was proposed by Lau and Bischof [18] and Miller and Astley [17], in which asymmetry comparison of the corresponding anatomical regions between the left and right breast images was performed in terms of shape, texture, and density. Lau and Bischof also proposed a directional feature to quantify oriented patterns. In the present work, we intend to concentrate upon disturbance in the normally symmetrical flow of structures in the breast.

4.1 Selection of the region of interest (ROI)

Figures 4 and 5 show the two pairs of images from the Mini-MIAS database [22] used in this work for illustration of the directional analysis procedure. Figures 4(a) and (b) are, respectively, the images mdb087 and mdb088 classified as a normal case. Figures 5(a) and (b) are the images mdb117 and mdb118 classified as an architectural distortion case.

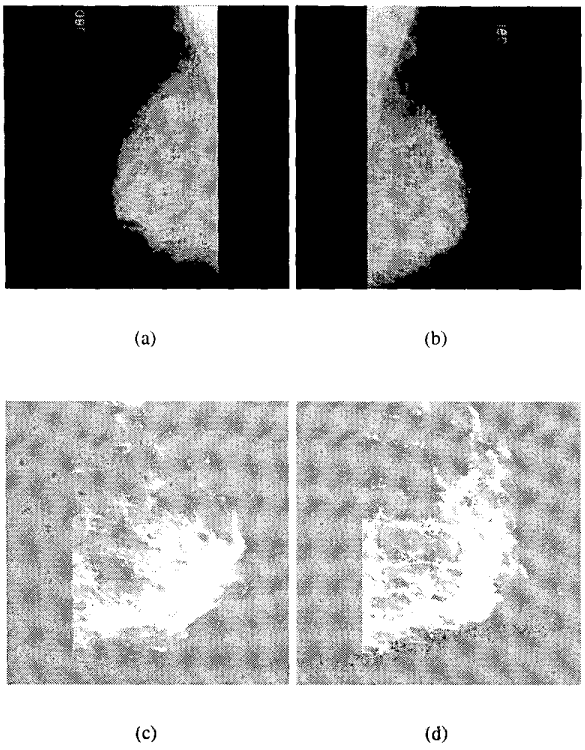

Figure 4: Images mdb087 and mdb088 of a normal case. (a) and (b) Original images. (c) and (d) Fibro–glandular disc segmented and enlarged. Histogram equalization was applied to enhance the global contrast of each ROI. The left ROI image (c) is flipped (mirrored) for easier comparison.

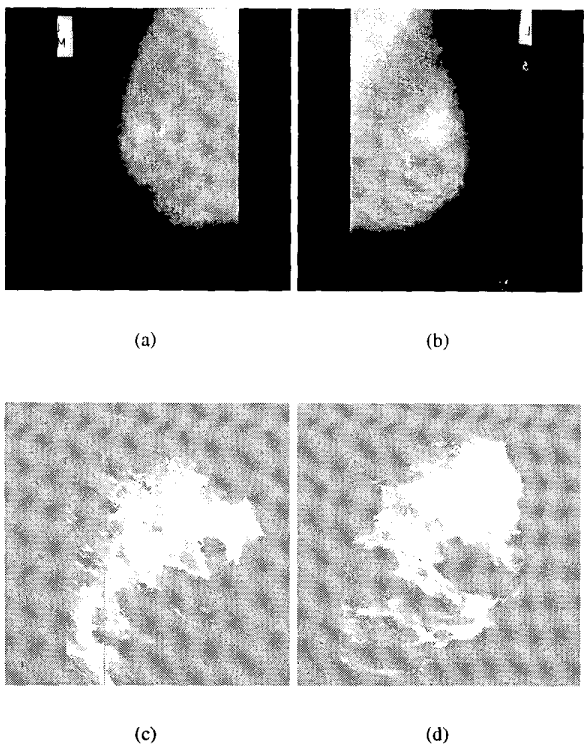

Figure 5: Images mdb117 and mdb118 of a case with architectural distortion. (a) and (b) Original images. (c) and (d) Fibro–glandular disc segmented and enlarged. Histogram equalization was applied to enhance the global contrast of each ROI. The left ROI image (c) is flipped (mirrored) for easier comparison.

In this work, we use only the fibro–glandular disc as the ROI in order to compute the directional components, due to the fact that most of the directional components such as connective tissues and ligaments occur in this specific region of the breast. The fibro–glandular disc is commonly localized near the nipple, and spreads through the interior of the breast until near the chest wall. Radiologists have noted that developing cancers are more often associated with glandular tissue than with fat [23]. When a tumor occurs in the fibro–glandular disc region of the breast, the natural directional flow of the tissues converging to the nipple changes locally in terms of orientation. Thus, a careful analysis of the directional components in the fibro–glandular disc can provide important information to radiologists.

In order to segment the fibro–glandular disc, we use a method that we have proposed [24] based upon the information in the gray–level intensity distribution to estimate a statistical model representing the fat and glandular tissues in the image. The statistical method used is the maximum–likelihood method with the probability density function represented by a Gaussian–mixture model. The parameters of the model are estimated by using the Expectation Maximization algorithm.

4.2 Feature extraction

In order to characterize asymmetry in mammograms, we use three features of directional distribution obtained from a Rose diagram that represents the difference between the Rose diagrams computed for the left and right mammograms. The Rose diagram or angle histogram is a graphical representation of directional information. In this representation, the area of each angle bin is proportional to the amount of information present in that specific direction.

The areas covered by each Rose diagram (left and right) were computed, and the maximum value used to normalize each angle bin of the Rose diagrams. This normalization permits a direct comparison of the left-breast and right-

breast Rose diagrams. The features used in the present work are described below.

a) Entropy (H) is used to represent the scatter of the directional components in an image. If the image is composed of directional components with a uniform distribution, the entropy value will be maximum; on the other hand, if the image is composed of directional components oriented in a very narrow angle band, the entropy value will be small. The entropy measure is computed as

$$H = -\sum_{i=1}^{N} x_i \log_2 x_i \ , \tag{5}$$

where N is the number of angle bins in the Rose diagram ($N = 12$ in the present work) and x_i is the ratio of the area of the directional components in the direction i to the total area represented by the Rose diagram.

b) The first–order angular moment (M_1) or mean orientation (θ) of an angular distribution is defined as

$$M_1 = \sum_{i=1}^{N} \theta_i x_i \ , \tag{6}$$

where θ_i is the central angle of the i^{th}angle band.

c) The second–order central moment (M_2) is a measure of the angular dispersion or variance computed with respect to the mean orientation as

$$M_2 = \sum_{i=1}^{N} (\theta_i - \bar{\theta})^2 x_i \ . \tag{7}$$

4.3 Pattern classification

Classification of the normal and asymmetric cases was conducted by using the Bayesian linear classifier [25]. The Gaussian distribution was assumed in order to model the probability density function (p.d.f), and the parameters of the model (mean vector $\overline{\mu}$ and covariance matrix Σ) were estimated by using the training samples. The prior probabilities of normal and asymmetric classes were assumed to be equal ($P_n = P_a = 0.5$), and the covariance matrix Σ was calculated in a pooled manner by averaging the covariance matrices of the normal and symmetric classes ($\Sigma = (\Sigma_i + \Sigma_j)/2$) . Thus, the statistical decision is made as

$$f(\overline{x}|w_i) \gtrless_{w_j}^{w_i} f(\overline{x}|w_j) \ , \tag{8}$$

$$f(\overline{x}|w_i) = \exp[-\frac{1}{2}(\overline{x} - \overline{\mu_i})^T \Sigma^{-1} (\overline{x} - \overline{\mu_i})] \ , \tag{9}$$

where w_i and w_j represent, respectively, the normal and asymmetric classes, and $f(\overline{x}|w_i)$ is the p.d.f. of the feature vector $\overline{x}$ in the class w_i.

The leave–one–out methodology [25] was used to estimate the classification accuracy since the number of samples used in this work is relatively small.

5 Results

The directional analysis scheme proposed was applied to 80 images (20 normal cases, 14 asymmetry cases, and 6 architectural distortion cases) from the Mini–MIAS database [22]. All images were medio-lateral oblique views with 200 μm sampling interval and 8-bit gray–level quantization.

Although the Gabor filters were implemented to provide good computing performance, the filtering process involves the computation of $S \times K$ Fast Fourier Transforms (FFT) and $S \times K$ inverse FFTs, where S and K are, respectively, the number of scales and orientations used in the filters. In the present work, $S = 4$ and $K = 12$, and all the filters were initially created in the spatial domain. Processing an image with a resolution of 512×512 pixels (size of the ROI) on a 450 MHz Pentium processor with 184 MB of memory took about 20 minutes.

Figure 6 shows the principal components obtained by applying the KL transform to the filter outputs for orientation 135^o and four scales. It can be seen that the relevant information is concentrated in the first two principal components. This is evident based on the evaluation of the eigenvalues, listed in the caption of Figure 6. In this example, only the first two principal components were used to represent the oriented components in the 135^o orientation, since their eigenvalues add to 99.11% ($> 95\%$) of the total variance.

After thresholding the filtered images with Otsu's method, in order to eliminate the effects of spectral leakage, the magnitude and phase images were composed by vector summation, as illustrated in Figures 7 and 8.

Figures 7(a)-(d) show the magnitude and phase images for the normal case in Figure 4. From the phase images, it is readily seen that the left and right views have almost the same dominant orientation. Some artifacts may be noticed in the chest wall region, caused by the gray–level transitions (see Figures 4(c) and (d)); the artifacts need to be removed in future works. The Rose diagrams in Figures 7(e) and (f) show the distribution of the tissues in the fibro–glandular disc of both the left and right views. An inspection of the Rose diagrams shows that the results obtained are in good agreement with visual analysis of the filtered results in Figures 7(c) and (d), and the corresponding ROIs in Figures 4(c) and (d). The most relevant global angular information indicated in the Rose diagrams are very similar.

The results of the filtering process for the architectural distortion case along with the respective Rose diagrams are shown in Figure 8. By analyzing the magnitude and phases images we can notice a modification of the tissue pattern

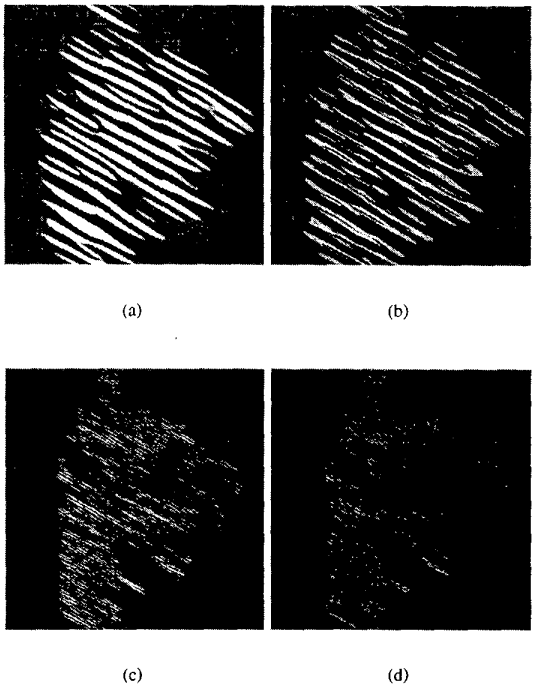

(a) (b)

(c) (d)

Figure 6: The images (a), (b), (c) and (d) are, respectively, the 1st, 2nd, 3rd, and 4th components resulting from the KL transform applied to the filter responses with orientation 135^o to the ROI of the image mdb117 shown in Figure 5(c). The eigenvalues of the four components above are: $\lambda_1 = 11.810541$, $\lambda_2 = 1.395799$, $\lambda_3 = 0.104770$, and $\lambda_4 = 0.012854$.

caused by the presence of a high-density region. An important characteristic of the Gabor filters may be seen in the result: the filters do not respond to regions with nearly uniform intensity, i.e., to regions without directional information. This is an important point and should be used in future works to detect asymmetric dense regions. In the present example, the global distribution of the tissue flow pattern is readily seen by comparison of the Rose diagrams.

The Rose diagrams in Figures 7 and 8 present a strong visual association with the directional components of the phase images obtained with the proposed method, and may be used by radiologists as an aid in mammogram interpretation.

Since we have used a small number of features, we applied an exhaustive combination approach in order to select the best set of features. The selection was conducted based on the classification results obtained by using the leave–one–out method. Preliminary results of the directional anal-

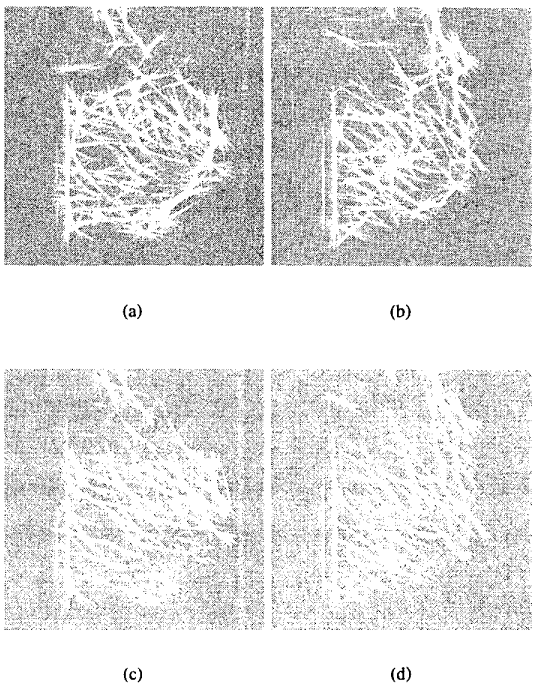

(a) (b)

(c) (d)

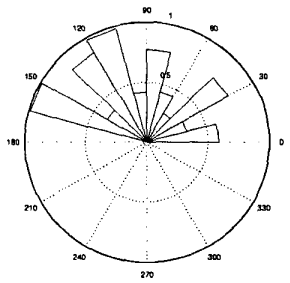

(e)

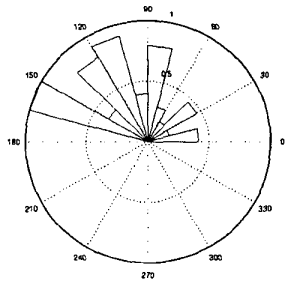

(f)

Figure 7: Results obtained for the the normal case in Figure 4. (a) and (b) magnitude images. (c) and (d) phase images. (e) and (f) Rose diagrams of the (c) and (d), respectively.

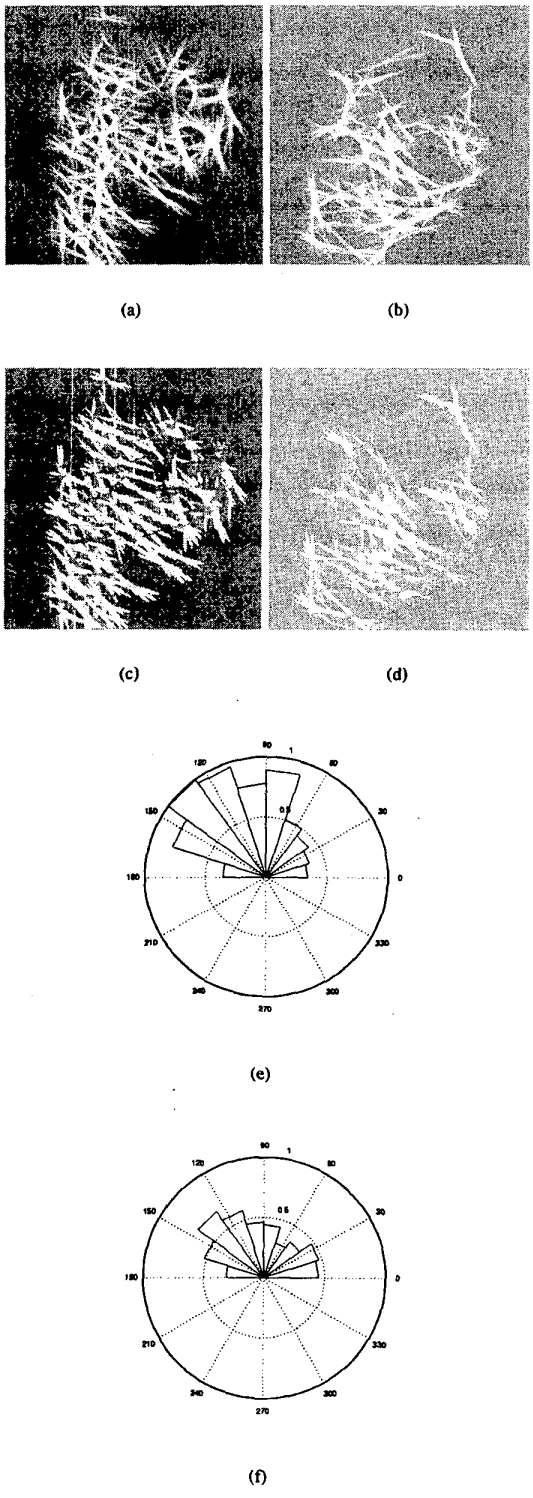

Figure 8: Results obtained for the the architectural distortion case in Figure 5. (a) and (b) magnitude images. (c) and (d) phase images. (e) and (f) Rose diagrams of the (c) and (d), respectively.

ysis procedure applied to differentiate pairs of normal mammograms from pairs of mammograms with asymmetry and architectural distortion by using the first–order angular moment (M_1) and the entropy (H) features indicate that 80% of the asymmetric and distortion cases, and 65% of the normal cases were correctly classified. The global rate of correct classification was 72.5%.

6 Discussion and Conclusions

The directional analysis procedure has proven to be an effective method for characterization of linear oriented components of images. Although the KL transform has been used to extract the most important components over the scales, the problem of automatic selection of the number of scales and orientation angles based on some optimality criterion needs to be solved. Further investigations should also be conduced to determine a more effective set of features for characterization of directional information.

The classification results are encouraging, considering the small number of features (first–order angular moment and entropy) used in this work to differentiate normal and asymmetric mammograms. We believe that further optimization of the directional analysis procedure along with an extensive investigation of new features can improve the results significantly. A more complete approach for the analysis of asymmetry must take into account other important characteristics, such as the shape of the fibro–glandular disc, asymmetric brightness, and texture differences. Features should also be investigated for measurement of local asymmetry. The method proposed in this work may eventually be applied to mammograms taken at different times in a screening program to detect interval cancer.

Acknowledgments

This project was supported by grants from Coordenação de Aperfeiçoamento de Pessoal de Ensino Superior (CAPES), Fundação de Amparo à Pesquisa de São Paulo (FAPESP), Brazil, and the Alberta Heritage Foundation for Medical Research (AHFMR), Alberta, Canada.

References

[1] Campbell FW and Robson JG. Application of Fourier analysis to the visibility of gratings. *Journal of Physiology*, 197:551–566, 1968.

[2] Marcelja S. Mathematical description of the response of simple cortical cells. *Journal of the Optical Society of America*, 70(11):1297–1300, 1980.

[3] Jones P and Palmer LA. An evaluation of the two-dimensional Gabor filter model of simple receptive

fields in cat striate cortex. *Journal of Neurophysiology*, 58(6):1233–1258, 1987.

[4] Daugman JG. Uncertainty relation for resolution in space, spatial frequency, and orientation optimized by two-dimensional visual cortical filters. *Journal of the Optical Society of America*, 2(7):1160–1169, 1985.

[5] Daugman JG. Complete discrete 2-D Gabor transforms by neural networks for image analysis and compression. *IEEE Transactions on Acoustics, Speech, and Signal Processing*, 36(7):1169–1179, 1988.

[6] Turner MR. Texture discrimination by Gabor functions. *Biological Cybernetics*, 55:71–82, 1986.

[7] Malik J and Perona P. Preattentive texture discrimination with early vision mechanisms. *Journal of the Optical Society of America A*, 7(2):923–932, 1990.

[8] Jain AK and Farrokhnia F. Unsupervised texture segmentation using Gabor filters. *Pattern Recognition*, 24(12):1167–1186, 1991.

[9] Dunn D, Higgins WE, and Wakeley J. Texture segmentation using 2-D Gabor elementary functions. *IEEE Transactions on Pattern Analysis and Machine Intelligence*, 16(2):130–149, 1994.

[10] Rolston WA and Rangayyan RM. Directional analysis of images using multi-resolution Gabor filters. In *Proceedings of International Conference on Robotics, Vision, and Parallel Processing for Industrial Vision*, pages 307–312, Ipoh, Malasia, May 1994.

[11] Bovik AC, Clark M, and Geisler WS. Multichannel texture analysis using localized spatial filters. *IEEE Transactions on Pattern Analysis and Machine Intelligence*, 12(1):55–73, 1990.

[12] Manjunath BS and Ma WY. Texture features for browsing and retrieval of image data. *IEEE Transactions on Pattern Analysis and Machine Intelligence*, 18(8):837–842, 1996.

[13] Jähne B. *Digital Image Processing*. Springer, San Diego, CA, 4th edition, 1997.

[14] Gonzalez RC and Woods RE. *Digital Image Processing*. Addison-Wesley, Reading, MA, 1992.

[15] Otsu N. A threshold selection method from gray-level histograms. *IEEE Transactions on Systems, Man, and Cybernetics*, SMC-9(1):62–66, 1979.

[16] Homer MJ. *Mammographic Interpretation: A Practical Approach*. McGraw-Hill, Boston, MA, 1997.

[17] Miller P and Astley S. Automated detection of mammographic asymmetry using anatomical features. *International Journal of Pattern Recognition and Artificial Intelligence*, 7(6):1461–1476, 1993.

[18] Lau TK and Bischof WF. Automated detection of breast tumors using the asymmetry approach. *Computers and Biomedical Research*, 24:273–295, 1991.

[19] Yin FF, Giger ML, Doi K, Vyborny CJ, and Schmidt RA. Computerized detection of masses in digital mammograms: automated alignment of breast images and its effect on bilateral-subtraction technique. *Medical Physics*, 21(3):445–452, 1994.

[20] Vujovic N and Brzakovic D. Establishing the correspondence between control points in pairs of mammographic images. *IEEE Transactions on Image Processing*, 6(10):1388–1399, 1997.

[21] Karssemeijer N and te Brake G. Combining single view features and asymmetry for detection of mass lesions. In Karssemeijer N, Thijssen M, Hendriks J, and van Erning L, editors, *Proceedings of the 4th International Workshop on Digital Mammography*, pages 95–102, Nijmegen, The Netherlands, June 1998.

[22] Suckling J, Parker J, Dance DR, Astley S, Hutt I, Boggis CRM, Ricketts I, Stamatakis E, Cerneaz N, Kok SL, Taylor P, Betal D, and Savage J. The Mammographic Image Analysis Society digital mammogram database. In Gale AG, Astley SM, Dance DR, and Cairns AY, editors, *Proceedings of the 2nd International Workshop on Digital Mammography*, pages 375–378, London, England, July 1994.

[23] Caulkin S, Astley S, Asquith J, and Boggis C. Sites of occurrence of malignancies in mammograms. In Karssemeijer N, Thijssen M, Hendriks J, and van Erning L, editors, *Proceedings of the 4th International Workshop on Digital Mammography*, pages 279–282, Nijmegen, The Netherlands, June 1998.

[24] Ferrari RJ, Rangayyan RM, Desautels JEL, and Frère AF. Segmentation of mammograms: Identification of the skin–air boundary, pectoral muscle, and fibro–glandular disc. In *Proceedings of the 5th International Workshop on Digital Mammography*, page in press, Toronto, Canada, June 2000.

[25] Duda RO and Hart PE. *Pattern Classification and Scene Analysis*. Wiley, New York, NY, 1973.